Engineering Science and Technology, an International Journal 21 (2018) 714–726

HOSTED BY

Contents lists available at ScienceDirect

Engineering Science and Technology, an International Journal

journal homepage: www.elsevier.com/locate/jestch

Full Length Article

Two-phase modeling of three-dimensional MHD porous flow of Upper-Convected Maxwell (UCM) nanofluids due to a bidirectional stretching surface: Homotopy perturbation method and highly nonlinear system of coupled equations

Amin Jafarimoghaddam [1]

Independent Researcher, Tehran, Iran

ARTICLE INFO

Article history:
Received 8 February 2018
Revised 22 May 2018
Accepted 5 June 2018
Available online 15 June 2018

Keywords:
Three-dimensional MHD flow
Maxwell nanofluids
Bidirectional stretching surface
Homotopy Perturbation Method

ABSTRACT

The present communication concerns with three-dimensional MHD/Porous flow of Maxwell nanofluids generated due to a bidirectional stretching surface in the presence of the Brownian motions of nanoparticles. The ability of Maxwell fluid model to capture the stress relaxation of some polymeric liquids together with the applications of stretching sheet flows in polymer industries shortly exhibit the importance of the subject matter. To this end, the associated conservative equations are initially converted to similarity forms. Here, by means of contemporary mathematics, it is presented an excellent and perhaps the simplest solution to the problem of interest in a generalized form for the first time. The distinctive attributes of the present paper can be summarized as:

1- Presenting the three-dimensional stretching flow of UCM fluid subject to a general consideration including nanoparticles Brownian motions, Darcy porosity and magnetic effects.
2- Analyzing the response of homotopy perturbation method to such nonlinearity.
3- A comprehensive report on the effects of the various engaged parameters.It is hopeful that the main features of such a fluid flow can be documented by means of the presented explicit analytic formulae and with the sufficiently provided figures which were hardly reachable until now.

1. Introduction

The past decade was an exhibition of various and sundry solutions (subject to different conditions) to stretching/shrinking sheet flows treated mainly analytically due to the reduction of the associated conservative equations in similarity forms for this particular geometry of flow. Applications of stretching sheet flows in pertinent industries is an encouraging factor which motivates researchers to develop mathematical models in order to give response to the industrial needs. In this regard, polymer industry stands as one of the major hosts for the solutions to stretching sheet flows, being associated with the fact that the extrusion of molten polymers precedes the development of plastic sheets in these industries. Besides, the applicability of nanofluids (base fluids with suspended nanoparticles) to enhancing heat transfer coefficient as an alternative to the usual traditional approaches may play a key role to achieve the purpose in the new world of emerging technologies (it is yet to be rigorously proven). Although literature is flourished in the two-dimensional solutions to stretching sheet flows, less attention has been paid to the three-dimensional cases.

In this communication, it is given a quick review on the most relevant previous studies regarding the three-dimensional stretching sheet flows.

Ariel gave an analytic solution to the three-dimensional flow of Newtonian fluids using Ackroyd method which is associated with the infinite series of negative exponentials [1]. It is to some extent mentioning that in [1], Ariel also gave perturbation solutions for small and large (close to unity) values of the dimensionless stretching ratio. He further presented an approximate solution using the method of trial functions and minimizing the connected residuals. Using the technique of Samuel and Hall, another solution was presented by Ariel in [2]. Hang Xu et al. [3] presented analytic solution to the three-dimensional magnetohydrodynamics (MHD)

[1] Previously at the Department of Aerospace Engineering, K. N. Toosi University of Technology, Tehran, Iran.
E-mail address: a.jafarimoghaddam@gmail.com.

Peer review under responsibility of Karabuk University.

https://doi.org/10.1016/j.jestch.2018.06.005
2215-0986/

flow of Newtonian fluids due to a bidirectional impulsively stretching surface by means of homotopy analysis method (HAM). Hayat and Javed [4] investigated the three-dimensional MHD flow of Newtonian fluids with transpiration velocity. They presented solutions obtained by HAM for the flow equations. As the main outcomes of that study, it was reported that injection type transpiration velocity suppresses the normalized skin friction coefficients whilst, suction increases the normalized wall shear factors. Furthermore, they recorded an enhancement for the normalized skin friction coefficients both by increasing the magnetic parameter and the dimensionless stretching ratio. Three- dimensional flow of viscoelastic fluids generated by a stretching surface was studied by Hayat et al. [5]. In that investigation, the associated similarity equations for momentum was treated via HAM. They gave report that the normalized skin friction factors escalate where both the material fluid parameter and the stretching ratio increase. More recently, three- dimensional flow of Maxwell fluids due a stretching surface was solved by Hayat and Awais [6] using HAM. They recorded an increase in the normalized wall shear factor with the increase of Deborah number. Three- dimensional flow of Oldroyd-B fluid subject to a convective boundary condition was analyzed by Hayat et al. [7]. The nonlinearity within the coupled equations was tackled using HAM. They have also provided some results for Nusselt number. Flow and heat transfer analysis of Maxwell nanofluids due to a bidirectional stretching surface was carried out in [8,9]. Specifically, in [8] authors have provided homotopic solutions (HAM) for evolution of velocity and temperature fields in the presence of an imposed magnetic field. This is whilst in [9] the engaged nonlinear equations were tackled using Runge–Kutta–Fehlberg fourth-fifth order scheme (RKF45 Method) along with shooting technique. There exist very marginal reports on the zeroth characteristics of momentum and energy equations in [8,9] which indeed are of the most significant outcomes required for the pertinent applications. This is of course due to the highly nonlinear nature of the associated conservative equations which somewhat prevents from proceeding further to obtain a structural solution. Unsteady flow of Maxwell fluids over a three- dimensional stretching surface was analyzed by Awais et al. [10]. In that study, authors applied HAM to generate convergent series solutions for momentum equations. The coupled equations of momentum subject to the flow of Jeffery fluid over a bidirectional stretching surface were solved using HAM in [11]. In that study, the effects of viscoelastic parameter as well as Deborah number on the evolution of velocity fields were evaluated for several cases. There exist several more studies on three-dimensional stretching sheet flows subject to different considerations such as Williamson fluids, exponentially stretching surface, variable thermal conductivity and so forth (for more information see e.g. [12–20]).

In view of the existing literature in this field, it is verified that all the solutions presented for three-dimensional stretching sheet flows of non-Newtonian fluids are numeric or of too lengthy analytic series expressions. Beyond the classical type solutions, it is presented in here a powerful structural solution to the problem of three-dimensional MHD/Porous flow of Maxwell nanofluids due to a bidirectional stretching surface where the thermophoresis effect is negligible. The solution is based on homotopy perturbation method (HPM) [21–23]. Although this topological algorithm has been mostly applied to the problems associated with one differential equation, here, it was examined and confirmed the suitability of the algorithm even if the problem is characterized by several highly non-linear differential equations. In this regard, it is first established a suitable homotopy to the momentum equations. The finalized solutions are shown to be of accurate ones which will be used further to tackle the remaining linear transport equations of energy and nanoparticles in a purely closed form manner.

In order to increase the accuracy, it is also applied the parameter expansion technique to obtain the 2nd order HPM solution. A comparison revealed that for the present nonlinearity the parameter expansion technique in its formal way relatively fails to provide considerably more accurate solutions. Therefore, for the sake of simplicity, the 1st order HPM solution was brought into account for further analysis. It should be mentioned that also the three-dimensional flow of UCM fluid has recently received some attentions from the researchers (as mentioned), but three major concerns are noted: 1- the reports on both the skin friction coefficient and the associated velocity profiles are insufficient 2- the effects of an imposed magnetic field and the porosity are almost missing 3- the associated thermal problem as well as the nanofluids considerations accounting two-phase modeling are rather untapped in the literature. Besides, the response of HPM with regard to a highly nonlinear system of coupled equations has not been extensively studied in the state of art. Therefore, the present research concerns with both a general consideration of a challenging problem in fluid dynamics and an application of HPM with respect to the resulting nonlinear system of coupled equations.

2. Mathematical model

Let us consider the three-dimensional, steady and incompressible MHD flow of upper-convected Maxwell liquid with suspended nanoparticles inside a porous medium generated via a bidirectional stretching surface (see Fig. 1 which serves as the schematic of the problem). Further note that the slip mechanism connected to thermophoresis effect is ignored and only the Brownian motion is taken into account as the transport mechanism for nanoparticles (referred to the two-phase modeling of nanofluids initially proposed by Jacopo Buongiorno [24]). In addition, in order to save a more general scheme, surface transpiration velocity (suction/injection) is also considered.

Under these assumptions, the boundary layer approximate equations of mass, momentum, energy and concentration become (see Ref. [8,9,25,26]):

$$\frac{\partial u}{\partial x}+\frac{\partial v}{\partial y}+\frac{\partial w}{\partial z}=0 \tag{1}$$

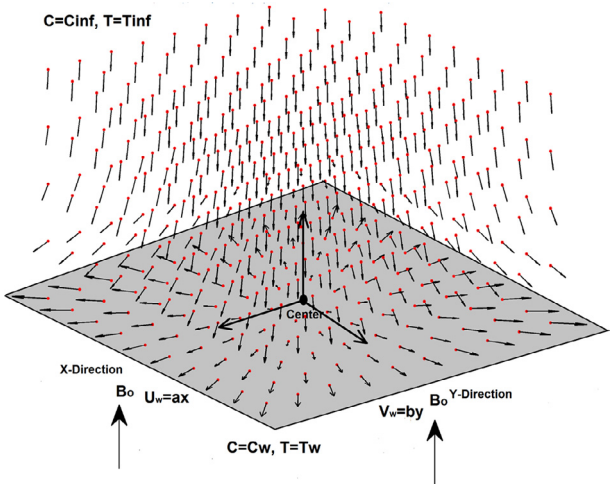

Fig. 1. Schematic of the problem (Solution by 1st order HPM obtained for axisymmetric bidirectional stretching flow of Newtonian fluids in the absence of porosity and magnetic effects): Above the surface, the space is assumed to be porous following the Darcy model. Additionally, the flowing fluid follows the non-Newtonian UCM fluid model containing suspended nanoparticles within.

$$u\frac{\partial u}{\partial x}+v\frac{\partial u}{\partial y}+w\frac{\partial u}{\partial z}+\lambda\begin{pmatrix}u^2\frac{\partial^2 u}{\partial x^2}+v^2\frac{\partial^2 u}{\partial y^2}+w^2\frac{\partial^2 u}{\partial z^2}+\\ 2uv\frac{\partial^2 u}{\partial x\partial y}+2vw\frac{\partial^2 u}{\partial y\partial z}+2uw\frac{\partial^2 u}{\partial x\partial z}\end{pmatrix}$$
$$=\upsilon\frac{\partial^2 u}{\partial z^2}-\frac{\sigma B_0^2}{\rho_f}\left(u+\lambda w\frac{\partial u}{\partial z}\right)-\frac{\upsilon}{\bar{K}}u \tag{2}$$

$$u\frac{\partial v}{\partial x}+v\frac{\partial v}{\partial y}+w\frac{\partial v}{\partial z}+\lambda\begin{pmatrix}u^2\frac{\partial^2 v}{\partial x^2}+v^2\frac{\partial^2 v}{\partial y^2}+w^2\frac{\partial^2 v}{\partial z^2}+\\ 2uv\frac{\partial^2 v}{\partial x\partial y}+2vw\frac{\partial^2 v}{\partial y\partial z}+2uw\frac{\partial^2 v}{\partial x\partial z}\end{pmatrix}$$
$$=\upsilon\frac{\partial^2 v}{\partial z^2}-\frac{\sigma B_0^2}{\rho_f}\left(v+\lambda w\frac{\partial v}{\partial z}\right)-\frac{\upsilon}{\bar{K}}v \tag{3}$$

$$u\frac{\partial T}{\partial x}+v\frac{\partial T}{\partial y}+w\frac{\partial T}{\partial z}=\alpha\frac{\partial^2 T}{\partial z^2}+\frac{(\rho c)_p}{(\rho c)_f}D_B\frac{\partial T}{\partial z}\frac{\partial C}{\partial z} \tag{4}$$

$$u\frac{\partial C}{\partial x}+v\frac{\partial C}{\partial y}+w\frac{\partial C}{\partial z}=D_B\frac{\partial^2 C}{\partial z^2} \tag{5}$$

Boundary conditions are supposed to be:

$$u=ax,\ v=by,\ w=W_0,\ T=T_w,\ C=C_w\ at\ z=0 \tag{6}$$

$$u\to 0,\ v\to 0,\ T\to T_\infty,\ C\to C_\infty\ as\ z\to\infty \tag{7}$$

In the above equations, u, v and w are velocity components in x, y and z directions respectively, λ the relaxation time, υ the kinematic viscosity, ρ_f the fluid density, σ electrical conductivity, B_0 the imposed magnetic field, $\bar{K}$ permeability of the porous medium, T temperature, α the thermal diffusivity, $(\rho c)_p$ and $(\rho c)_f$ the effective heat capacity of nanoparticles and fluid respectively, C concentration, D_B the Brownian diffusion coefficient, W_0 the suction/injection parameter, T_∞ and T_w temperatures far from the surface and at the surface respectively, C_∞ and C_w concentrations far from the surface and at the surface respectively. Furthermore, a and b are the stretching factors in "x" and "y" directions respectively.

Employing the following similarity quantities:

$$u=axf'(\eta),\ v=ayg'(\eta),\ w=-(a\upsilon)^{\frac{1}{2}}(f(\eta)+g(\eta))\theta$$
$$=\frac{T-T_\infty}{T_w-T_\infty},\ \phi=\frac{C-C_\infty}{C_w-C_\infty},\ \eta=\left(\frac{a}{\upsilon}\right)^{\frac{1}{2}}z \tag{8}$$

The finalized similarity equations are obtained as:

$$f'''(\eta)+(M\beta+1)(f(\eta)+g(\eta))f''(\eta)-f'(\eta)^2$$
$$+\beta\begin{pmatrix}2(f(\eta)+g(\eta))f'(\eta)f''(\eta)\\ -(f(\eta)+g(\eta))^2f'''(\eta)\end{pmatrix}-(M+K)f'(\eta)=0 \tag{9}$$

$$g'''(\eta)+(M\beta+1)(f(\eta)+g(\eta))g''(\eta)-g'(\eta)^2$$
$$+\beta\begin{pmatrix}2(f(\eta)+g(\eta))g'(\eta)g''(\eta)\\ -(f(\eta)+g(\eta))^2g'''(\eta)\end{pmatrix}-(M+K)g'(\eta)=0 \tag{10}$$

$$\theta''(\eta)+\mathrm{Pr}(f(\eta)+g(\eta))\theta'(\eta)+N_b\theta'(\eta)\phi'(\eta)=0 \tag{11}$$

$$\phi''(\eta)+Sc(f(\eta)+g(\eta))\phi'(\eta)=0 \tag{12}$$

The associated boundary conditions become:

$$f(0)+g(0)=R,f'(0)=1,g'(0)=c,\theta(0)=\phi(0)=1f'(\eta\to\infty)$$
$$=g'(\eta\to\infty)=\theta(\eta\to\infty)=\phi(\eta\to\infty)=0 \tag{13}$$

In Eqs. (9) to (13), M is magnetic parameter, K is the corresponding Darcian resistance parameter, β is Deborah number, c is the ratio of the stretching rates, R is suction/injection parameter, Pr is Prandtl number, N_b is Brownian parameter and Sc is Schmidt number. These parameters are defined as:

$$M=\frac{\sigma B_0^2}{\rho_f a},\ K=\frac{v}{\bar{K}a},\ \beta=\lambda a,\ c=\frac{b}{a},\ R=-\frac{W_0}{(a\upsilon)^{\frac{1}{2}}},\ \mathrm{Pr}=\frac{\upsilon}{\alpha},$$
$$N_b=\frac{(\rho c)_p D_B(C_w-C_\infty)}{(\rho c)_f\alpha},\ Sc=\frac{\upsilon}{D_B} \tag{14}$$

Note that $R>0$ corresponds to suction, whilst $R<0$ stands for the injection case.

Besides, Nusselt and Sherwood numbers are defined as:

$$Nu_x=-\frac{x}{T_w-T_\infty}\frac{\partial T}{\partial z}|z=0=-(\mathrm{Re}_x)^{\frac{1}{2}}\theta'(0)Sh_x$$
$$=-\frac{x}{C_w-C_\infty}\frac{\partial C}{\partial z}|z=0=-(\mathrm{Re}_x)^{\frac{1}{2}}\phi'(0) \tag{15}$$

Where $\mathrm{Re}_x=\frac{ux}{\upsilon}$

Obviously, when parameter c is set to zero, two-dimensional stretching scheme is recovered. Besides, letting c be equal to unity, the flow geometry takes an axisymmetric form. In addition, taking β as to be zero, Newtonian case is recovered. Furthermore, letting N_b be equal to zero, converts the nanofluids problem to the base fluids one.

3. Solution Strategy: 1st order HPM

As mentioned earlier, homotopy perturbation method of the 1st and the 2nd order are used to tackle the resulting similarity equations for momentum. Although the method has been mostly applied to problems dealing with only one differential equation, here by constructing a suitable homotopy, it is shown that this topological method may be promising even for highly nonlinear coupled equations.

Let us rewrite Eqs. (9) and (10) within the following homotopic forms:

$$f'''-(k^*)^2f'+p((M\beta+1)(f+g)f''-f'^2+\beta(2(f+g)f'f''$$
$$-(f+g)^2f''')-(M+K)f'+(k^*)^2f')=0 \tag{16}$$

$$g'''-(k^*)^2g'+p((M\beta+1)(f+g)g''-g'^2+\beta(2(f+g)g'g''$$
$$-(f+g)^2g''')-(M+K)g'+(k^*)^2g')=0 \tag{17}$$

Where $f=f(\eta)$, $g=g(\eta)$, p is the homotopy perturbation parameter and k^* is to be further determined through the solution procedure. When $p=0$, the system of above equations is reduced to simplified forms which in particular express the initial guess for the actual solution of interest. Besides, as the parameter p evolves to eventually take the value of unity, the original system of equations is readily recovered. Therefore, the initial solutions deform to reach the required ones through the evolution of homotopy perturbation parameter. In algebraic topology, this concept is called homotopy.

In view of the standard practice of homotopy perturbation method (HPM), the solutions are sought as:

$$f=f_0+pf_1+p^2f_2+\dots \tag{18}$$

$$g=g_0+pg_1+p^2g_2+\dots \tag{19}$$

Substituting Eqs. (18) and (19) in Eqs. (16) and Eq. (17) and equating the identical powers of p, the two first systems are deduced as:

$$f_0'''-(k^*)^2f_0'=0g_0'''-(k^*)^2g_0'=0f_0(0)+g_0(0)=R,f_0'(0)$$
$$=1,g_0'(0)=cf'(\infty)=0,g'(\infty)=0 \tag{20}$$

$$f_1''' - (k^*)^2 f_1' + (M\beta+1)(f_0+g_0)f_0'' - f_0'^2 + \beta(2(f_0+g_0)f_0'f_0'' - (f_0+g_0)^2 f_0''') - (M+K)f_0' + (k^*)^2 f_0' = 0 g_1''' - (k^*)^2 g_1' + (M\beta+1)(f_0+g_0)g_0'' - g_0'^2 + \beta(2(f_0+g_0)g_0'g_0'' - (f_0+g_0)^2 g_0''') - (M+K)g_0' + (k^*)^2 g_0' = 0 f_1(0) + g_1(0) = 0, f_1'(0) = 0, g_1'(0) = 0 f_1'(\infty) = 0, g_1'(\infty) = 0 \quad (21)$$

The auxiliary parameter k^* can be obtained via several routes. However, as it has been outlined by He [27], this parameter should be obtained in such a way that the finalized solutions are free from secular terms such as $\eta e^{-k^*\eta}$. Once the secular terms are removed, we have automatically truncated the degree of the series solutions and consequently lose control on the appearance of secular terms in higher order systems. However, there is almost no need for further series terms since over many practices in this field, the method has proven itself highly efficient even on using only the two first series terms. Therefore, we may write:

$$f = f_0 + f_1 \quad (22)$$

$$g = g_0 + g_1 \quad (23)$$

We solve systems (20) and (21), remove the secular term $\eta e^{-k^*\eta}$ and obtain with ease (simplified, so that they can be easily applied and followed):

$$f(\eta) + g(\eta) = R + \frac{1}{k^*}(1+c)(1-e^{-k^*\eta}) + (A_1 + A_3 + 2A_2 + 2A_4) - (2(A_1+A_3) + 3(A_2+A_4))e^{-k^*\eta} + (A_1+A_3)e^{-2k^*\eta} + (A_2+A_4)e^{-3k^*\eta} \quad (24)$$

$$f'(\eta) = (1 + (2A_1 + 3A_2)k^*)e^{-k^*\eta} + (-2k^*A_1)e^{-2k^*\eta} + (-3k^*A_2)e^{-3k^*\eta} \quad (25)$$

$$g'(\eta) = (c + (2A_3 + 3A_4)k^*)e^{-k^*\eta} + (-2k^*A_3)e^{-2k^*\eta} + (-3k^*A_4)e^{-3k^*\eta} \quad (26)$$

$$f''(0) = -k^* + (k^*)^2(2A_1 + 6A_2) \quad (27)$$

$$g''(0) = -ck^* + (k^*)^2(2A_3 + 6A_4) \quad (28)$$

$$A_1 = \frac{2\beta(1+c) - 2\beta(1+c)^2 + 1 - (1+M\beta)(1+c) - 2Rc\beta k^*}{-6(k^*)^3} \quad (29)$$

$$A_2 = \frac{\beta(1+c)^2 - 2\beta(1+c)}{-24(k^*)^3} \quad (30)$$

$$A_3 = \frac{2\beta c^2(1+c) - 2\beta c(1+c)^2 + c^2 - (1+M\beta)c(1+c) - 2Rc\beta k^*}{-6(k^*)^3} \quad (31)$$

$$A_4 = \frac{\beta c(1+c)^2 - 2\beta c^2(1+c)}{-24(k^*)^3} \quad (32)$$

$$k^* = \frac{-R((1+M\beta) + 2\beta(1+c))}{2(R^2\beta - 1)} \pm \frac{\left(R^2((1+M\beta) + 2\beta(1+c))^2 - 4(R^2\beta - 1)\begin{pmatrix}(1+M\beta)(1+c)+\\ \beta(1+c)^2 + (M+K)\end{pmatrix}\right)^{\frac{1}{2}}}{2(R^2\beta - 1)} \quad (33)$$

According to Eq. (33), it is readily observable that considering a transpiration velocity of either suction or injection type enters complexity into the solution. The complexity refers to both imposing a band in which the strategy yields physical solutions and even possible appearance of dual solutions with respect to ± sign which should be checked for triviality or stability. Therefore, in order to stay with the scope of the present communication and further to study a more realistic problem, we shall leave the suction/injection cases for future researches. With $R = 0$, a unique and unconditional solution is obtained where:

$$k^* = \sqrt{((1+M\beta)(1+c) + \beta(1+c)^2 + (M+K))} \quad (34)$$

4. A Trial with the Parameter Expansion Technique ($R = 0$): 2nd Order HPM

Let us rewrite Eqs. (9) and (10) in the following forms:

$$f''' + (-(k_1^*)^2 + k_2^* p)f' + p((M\beta+1)(f+g)f'' - f'^2 + \beta(2(f+g)f'f'' - (f+g)^2 f''') - (M+K)f' - (-(k_1^*)^2 + k_2^* p)f') = 0 \quad (35)$$

$$g''' + (-(k_1^*)^2 + k_2^* p)g' + p((M\beta+1)(f+g)g'' - g'^2 + \beta(2(f+g)g'g'' - (f+g)^2 g''') - (M+K)g' - (-(k_1^*)^2 + k_2^*)g') = 0 \quad (36)$$

Again on using straightforward expansion (Taylor Method) the above systems are expressed as:

$$f_0''' - (k_1^*)^2 f_0' = 0 g_0''' - (k_1^*)^2 g_0' = 0 f_0(0) + g_0(0) = 0, f_0'(0) = 1, g_0'(0) = cf'(\infty) = 0, g'(\infty) = 0 \quad (37)$$

$$f_1''' - (k_1^*)^2 f_1' + (M\beta+1)(f_0+g_0)f_0'' - f_0'^2 + \beta(2(f_0+g_0)f_0'f_0'' - (f_0+g_0)^2 f_0''') - (M+K)f_0' + ((k_1^*)^2 + k_2^*)f_0' = 0 g_1''' - (k_1^*)^2 g_1' + (M\beta+1)(f_0+g_0)g_0'' - g_0'^2 + \beta(2(f_0+g_0)g_0'g_0'' - (f_0+g_0)^2 g_0''') - (M+K)g_0' + ((k_1^*)^2 + k_2^*)g_0' = 0 f_1(0) + g_1(0) = 0, f_1'(0) = 0, g_1'(0) = 0 f_1'(\infty) = 0, g_1'(\infty) = 0 \quad (38)$$

$$f_2''' - (k_1^*)^2 f_2' + (M\beta+1)((f_0+g_0)f_1'' + (f_1+g_1)f_0'') - (2f_0'f_1') + \beta(2((f_0+g_0)f_0'f_1'' + (f_0+g_0)f_1'f_0'' + (f_1+g_1)f_0'f_0'') - ((f_0+g_0)(f_0+g_0)f_1''' + 2(f_0+g_0)(f_1+g_1)f_0''')) - (M+K)f_1' + ((k_1^*)^2 + k_2^*)f_1' - k_2^* f_0' = 0 g_2''' - (k_1^*)^2 g_2' + (M\beta+1)((f_0+g_0)g_1'' + (f_1+g_1)g_0'') - (2g_0'g_1') + \beta(2((f_0+g_0)g_0'g_1'' + (f_0+g_0)g_1'g_0'' + (f_1+g_1)g_0'g_0'') - ((f_0+g_0)(f_0+g_0)g_1''' + 2(f_0+g_0)(f_1+g_1)g_0''')) - (M+K)g_1' + ((k_1^*)^2 + k_2^*)g_1' - k_2^* g_0' = 0 f_2(0) + g_2(0) = 0, f_2'(0) = 0, g_2'(0) = 0 f_2'(\infty) = 0, g_2'(\infty) = 0 \quad (39)$$

After solving the above systems, removing the occurring secular terms it is obtained with ease:

$$L = \beta + 4c + 2M\beta + 15\beta c + 4M\beta^2 + 15\beta c^2 + 16\beta^2 c + \beta c^3 + 2\beta^2 + 28\beta^2 c^2 + 16\beta^2 c^3 + 2\beta^2 c^4 + 12M\beta^2 c^2 + 4M\beta^2 c^3 + 4M\beta c + 2M\beta c^2 + 12M\beta^2 c \quad (40)$$

$$Q = 24\beta c + 12M\beta c + 12M\beta + 12K + 12M + 12\beta + 12c + 12 + 12\beta c^2 \tag{41}$$

$$P = -12 \tag{42}$$

$$k_1^* = \sqrt{\frac{(-Q - \sqrt{Q^2 - 4PL})}{2P}} \tag{43}$$

$$k_2^* = K + M + \beta + c + M\beta + 2\beta c + \beta c^2 - (k_1^*)^2 + M\beta c + 1 \tag{44}$$

$$\sum_{i=0}^{2} f_i''(0) = \frac{\begin{vmatrix} 180K^2 + 80KM\beta c + 80KM\beta + 360KM + 60K\beta c^2 + 240K\beta c + 180K\beta - 1080K(k_1^*)^2 - \\ 360Kk_2^* + 120Kc + 360K - 20M^2\beta^2c^2 - 40M^2\beta^2c - 20M^2\beta^2 + 80M^2\beta c + 80M^2\beta + \\ 180M^2 - 22M\beta^2c^3 - 54M\beta^2c^2 - 42M\beta^2c - 10M\beta^2 - 320M\beta(k_1^*)^2c - 320M\beta(k_1^*)^2 - \\ 80M\beta k_2^*c - 80M\beta k_2^* + 40M\beta c^2 + 280M\beta c + 240M\beta - 1080M(k_1^*)^2 - 360Mk_2^* + \\ 120Mc + 360M + 17\beta^2c^4 + 24\beta^2c^3 - 6\beta^2c^2 + 8\beta^2c + 21\beta^2 - 180\beta(k_1^*)^2c^2 - 720\beta(k_1^*)^2c \\ -540\beta(k_1^*)^2 - 60\beta k_2^*c^2 - 240\beta k_2^*c - 180\beta k_2^* + 30\beta c^3 + 62\beta c^2 + 162\beta c + 162\beta - 540(k_1^*)^4 \\ +360(k_1^*)^2k_2^* - 360(k_1^*)^2c - 1080(k_1^*)^2 + 180(k_2^*)^2 - 120k_2^*c - 360k_2^* + 20c^2 + 80c + 180 \end{vmatrix}}{1440(k_1^*)^3} \tag{45}$$

$$\sum_{i=0}^{2} g_i''(0) = c\frac{\begin{vmatrix} 180K^2 + 80KM\beta c + 80KM\beta + 360KM + 180K\beta c^2 + 240K\beta c + 60K\beta - 1080K(k_1^*)^2 \\ -360Kk_2^* + 360Kc + 120K - 20M^2\beta^2c^2 - 40M^2\beta^2c - 20M^2\beta^2 + 80M^2\beta c + 80M^2\beta \\ +180M^2 - 10M\beta^2c^3 - 42M\beta^2c^2 - 54M\beta^2c - 22M\beta^2 - 320M\beta(k_1^*)^2c - 320M\beta + 80c \\ (k_1^*)^2 - 80M\beta k_2^*c - 80M\beta k_2^* + 240M\beta c^2 + 280M\beta c + 40M\beta - 1080M(k_1^*)^2 - 360 + 20 \\ Mk_2^* + 360Mc + 120M + 21\beta^2c^4 + 8\beta^2c^3 - 6\beta^2c^2 + 24\beta^2c + 17\beta^2 - 540\beta(k_1^*)^2c^2 - 720 \\ \beta(k_1^*)^2c - 180\beta(k_1^*)^2 - 180\beta k_2^*c^2 - 240\beta k_2^*c - 60\beta k_2^* + 162\beta c^3 + 162\beta c^2 + 62\beta c + 30 \\ \beta - 540(k_1^*)^4 + 360(k_1^*)^2k_2^* - 1080(k_1^*)^2c - 360(k_1^*)^2 + 180(k_2^*)^2 - 360k_2^*c - 120k_2^* + 180c^2 \end{vmatrix}}{1440(k_1^*)^3} \tag{46}$$

$$f_0(\eta) + g_0(\eta) = -(1+c)\frac{(e^{(-k_1^*\eta)} - 1)}{k_1^*} \tag{47}$$

$$f_1(\eta) + g_1(\eta) = \frac{1}{24(k_1^*)^3}e^{(-3k_1^*\eta)}(e^{(k_1^*\eta)} - 1)^2\left(\beta - \beta c - \beta c^2 + \beta c^3 + \begin{pmatrix} 2\beta + 8c + 14\beta c^2 + 2\beta c^3 + 4M\beta \\ +14\beta c + 8M\beta c + 4M\beta c^2 \end{pmatrix}e^{(k_1^*\eta)}\right) \tag{48}$$

$$f_2(\eta) + g_2(\eta) = -\frac{1}{2880(k_1^*)^5}e^{(-5k_1^*\eta)}(e^{(k_1^*\eta)} - 1)\begin{pmatrix} (7\beta^2c + 3\beta^2 - 10\beta^2c^2 - 10\beta^2c^3 + 7\beta^2c^4 + 3\beta^2c^5) \\ +A_1e^{k_1^*\eta} + A_2e^{2k_1^*\eta} + A_3e^{3k_1^*\eta} + A_4e^{4k_1^*\eta} \end{pmatrix} \tag{49}$$

$$A_1 = \begin{pmatrix} -8\beta - 61\beta^2 - 50M\beta^2 + 144\beta c^2 + 7\beta^2c + 32\beta c^3 - 8\beta c^4 + 438\beta^2c^2 + 438\beta^2c^3 \\ +7\beta^2c^4 - 61\beta^2c^5 + 32\beta c + 96M\beta^2c + 96M\beta^2c^3 + 292M\beta^2c^2 - 50M\beta^2c^4 \end{pmatrix} \tag{50}$$

$$A_2 = \begin{pmatrix} -20M\beta^2c^4 - 1184M\beta^2c^3 - 240M^2\beta^2c - 2328M\beta^2c^2 - 20M\beta c^3 - 1184M\beta^2c - 380M\beta c^2 \\ -80M^2\beta^2c^3 - 240M^2\beta^2c^2 - 380M\beta c - 608\beta c - 20M\beta + 104\beta^2c^5 - 688\beta^2c^4 - 2872\beta^2c^3 - \\ 2872\beta^2c^2 - 80M^2\beta^2 + 22\beta c^4 - 608\beta c^3 - 688\beta^2c + 22\beta - 120c + 104\beta^2 - 120c^2 - 20M\beta^2 - 1516\beta c^2 \end{pmatrix} \tag{51}$$

$$A_3 = \begin{pmatrix} 520M\beta^2c^4 + 3616M\beta^2c^3 + 720M^2\beta^2c + 6192M\beta^2c^2 + 140M\beta c^3 + 3616M\beta^2c + 1380M\beta c^2 + 22\beta \\ +240M^2\beta^2c^3 + 720M^2\beta^2c^2 + 1380M\beta c + 2272\beta c + 140M\beta + 104\beta^2c^5 + 2672\beta^2c^4 + 7848\beta^2c^3 \\ +7848\beta^2c^2 + 240M^2\beta^2 + 22\beta c^4 + 2272\beta c^3 + 2672\beta^2c + 4884\beta c^2 + 520M\beta^2 + 520c^2 + 104\beta^2 + 520c \end{pmatrix} \tag{52}$$

$$A_4 = \begin{pmatrix} +2880M\beta(k_1^*)^2c + 1440M\beta(k_1^*)^2c^2 + 1440\beta(k_1^*)^2c^3 + 4320\beta(k_1^*)^2c^2 + 30M\beta^2c^4 + 224\beta c \\ -480M^2\beta^2c - 1276M\beta^2c^2 + 4320\beta(k_1^*)^2c + 1440M(k_1^*)^2c + 120M\beta c^3 - 608M\beta^2c \\ -280M\beta c^2 + 1440M\beta(k_1^*)^2 + 1440K(k_1^*)^2c - 160M^2\beta^2c^3 - 480M^2\beta^2c^2 - 280M\beta c + \\ 120M\beta + 1440(k_1^*)^2c^2 + 90\beta^2c^5 + 162\beta^2c^4 - 124\beta^2c^3 - 124\beta^2c^2 - 160M^2\beta^2 - 1440(k_1^*)^4c + \\ +84\beta c^4 + 224\beta c^3 + 162\beta^2c + 1440K(k_1^*)^2 + 88\beta c^2 + 1440\beta(k_1^*)^2 + 1440M(k_1^*)^2 + 30M\beta^2 \\ +1440(k_1^*)^2 + 90\beta^2 + 2880(k_1^*)^2c + 84\beta + 80c^2 - 1440(k_1^*)^4 + 80c - 608M\beta^2c^3 + 140M\beta c^3 \end{pmatrix} \tag{53}$$

$$f_0'(\eta) = e^{(-k_1^*\eta)} \tag{54}$$

$$f_1'(\eta)=\frac{1}{24(k_1^*)^2}e^{(-3k_1^*\eta)}(e^{(k_1^*\eta)}-1)\begin{pmatrix}3\beta+3\beta e^{(k_1^*\eta)}+8ce^{(k_1^*\eta)}-3\beta c^2+13\beta c^2e^{(k_1^*\eta)}\\+8M\beta e^{(k_1^*\eta)}+16\beta ce^{(k_1^*\eta)}+8M\beta ce^{(k_1^*\eta)}\end{pmatrix} \tag{55}$$

$$f_2'(\eta)=\frac{1}{2880(k_1^*)^4}e^{(-5k_1^*\eta)}(e^{(k_1^*\eta)}-1)\begin{pmatrix}+160\beta^2c+15\beta^2+110\beta^2c^2-160\beta^2c^3-125\beta^2c^4\\+A_1e^{k_1^*\eta}+A_2e^{2k_1^*\eta}+A_3e^{3k_1^*\eta}\end{pmatrix} \tag{56}$$

$$A_1=\begin{pmatrix}-768\beta^2c+288\beta c^2-200M\beta^2-32\beta-241\beta^2+320\beta c^3+206\beta^2c^2\\+1536\beta^2c^3+803\beta^2c^4-192\beta c-8M\beta^2c+392M\beta^2c^3+584M\beta^2c^2\end{pmatrix} \tag{57}$$

$$A_2=\begin{pmatrix}-1618M\beta^2c^3-480M^2\beta^2c-3346M\beta^2c^2-1838M\beta^2c-540M\beta c^2-1762\beta^2c^4\\-240M^2\beta^2c^2-600M\beta c-462\beta c-4704\beta^2c^3-3484\beta^2c^2+58\beta-60M\beta\\-120c+254\beta^2-240c^2-110M\beta^2-2202\beta c^2-288\beta^2c-1330\beta c^3-240M^2\beta^2\end{pmatrix} \tag{58}$$

$$A_3=\begin{pmatrix}+2102M\beta^2c^3+800M^2\beta^2c+5174M\beta^2c^2+4042M\beta^2c+1060M\beta c^2+970M\beta^2\\+400M^2\beta^2c^2+1320M\beta c+2418\beta c+260M\beta+1598\beta^2c^4+6016\beta^2c^3+400c^2\\+7236\beta^2c^2+400M^2\beta^2+1550\beta c^3+3072\beta^2c+4198\beta c^2+58\beta+520c+254\beta^2\end{pmatrix} \tag{59}$$

Finally:

$$f'(\eta)=f_0'(\eta)+f_1'(\eta)+f_2'(\eta) \tag{60}$$

Similarly:

$$g_0'(\eta)=ce^{(-k_1^*\eta)} \tag{61}$$

$$g_1'(\eta)=\frac{c}{24(k_1^*)^2}e^{(-3k_1^*\eta)}(e^{(k_1^*\eta)}-1)\begin{pmatrix}8e^{(k_1^*\eta)}-3\beta+13\beta e^{(k_1^*\eta)}+3\beta c^2+3\beta c^2e^{(k_1^*\eta)}+\\8M\beta e^{(k_1^*\eta)}+16\beta ce^{(k_1^*\eta)}+8M\beta ce^{(k_1^*\eta)}\end{pmatrix} \tag{62}$$

$$g_2'(\eta)=\frac{c}{2880(k_1^*)^4}e^{(-5k_1^*\eta)}(e^{(k_1^*\eta)}-1)\begin{pmatrix}-160\beta^2c-125\beta^2+110\beta^2c^2+160\beta^2c^3+15\beta^2c^4\\+A_1e^{k_1^*\eta}+A_2e^{2k_1^*\eta}+A_3e^{3k_1^*\eta}\end{pmatrix} \tag{63}$$

$$A_1=\begin{pmatrix}-8M\beta^2c^2-200M\beta^2c^3+584M\beta^2c+288\beta c-768\beta^2c^3-241\beta^2c^4+\\206\beta^2c^2-32\beta c^3+1536\beta^2c-192\beta c^2+320\beta+803\beta^2+392M\beta^2\end{pmatrix} \tag{64}$$

$$A_2=\begin{pmatrix}-110M\beta^2c^3-480M^2\beta^2c-1838M\beta^2c^2-3346M\beta^2c-60M\beta c^2-240M^2\beta^2c^2\\-600M\beta c-2202\beta c-1762\beta^2-240-1330\beta+254\beta^2c^4+254\beta^2c^4-540M\beta-\\288\beta^2c^3-3484\beta^2c^2-240M^2\beta^2+58\beta c^3-4704\beta^2c-462\beta c^2-1618M\beta^2-120c\end{pmatrix} \tag{65}$$

$$A_3=\begin{pmatrix}+970M\beta^2c^3+800M^2\beta^2c+4042M\beta^2c^2+5174M\beta^2c+260M\beta c^2+400M^2\beta^2c^2\\+1320M\beta c+4198\beta c+1060M\beta+254\beta^2c^4+3072\beta^2c^3+7236\beta^2c^2+400M^2\beta^2\\+58\beta c^3+6016\beta^2c+2418\beta c^2+2102M\beta^2+1598\beta^2+520c+400+1550\beta\end{pmatrix} \tag{66}$$

Finally:

$$g'(\eta)=g_0'(\eta)+g_1'(\eta)+g_2'(\eta) \tag{67}$$

Having $f(\eta)+g(\eta)$ known from Eq. (24) or Eqs. (47)–(53), Eqs. (11) and (12) can be simply solved explicitly through the following closed form integral manners (which can be easily quantified directly by numerical integration):

$$\theta(\eta)=1+\theta'(0)\vartheta(\eta),\ \vartheta(\eta)=\int_0^\eta e^{-\Pr\left(\int_0^\eta(f(\eta)+g(\eta))\,d\eta\right)-N_b\phi'(0)\left(\int_0^\eta e^{-Sc\int_0^\eta(f(\eta)+g(\eta))\,d\eta}d\eta\right)}d\eta,\ \theta'(0)=\frac{-1}{\vartheta(\infty)} \tag{68}$$

$$\phi(\eta)=1+\phi'(0)\varphi(\eta),\ \varphi(\eta)=\int_0^\eta e^{-Sc\int_0^\eta(f(\eta)+g(\eta))\,d\eta}d\eta,\ \phi'(0)=\frac{-1}{\varphi(\infty)} \tag{69}$$

For example, on using Eqs. (24), (68) and (69) can be further simplified to yield:

$$\vartheta(\eta)=\int_0^{\eta}\frac{e^{-\Pr\left(R\eta+\frac{1}{k^*}(1+c)\eta+\frac{1}{(k^*)^2}(1+c)e^{-k^*\eta}+(A_1+A_3+2A_2+2A_4)\eta+\frac{1}{k^*}(2(A_1+A_3)+3(A_2+A_4))e^{-k^*\eta}-\frac{1}{2k^*}(A_1+A_3)e^{-2k^*\eta}-\frac{1}{3k^*}(A_2+A_4)e^{-3k^*\eta}\right)_0^{\eta}}}{e^{N_b\phi'(0)\int_0^{\eta}e^{-Sc\left(R\eta+\frac{1}{k^*}(1+c)\eta+\frac{1}{(k^*)^2}(1+c)e^{-k^*\eta}+(A_1+A_3+2A_2+2A_4)\eta+\frac{1}{k^*}(2(A_1+A_3)+3(A_2+A_4))e^{-k^*\eta}-\frac{1}{2k^*}(A_1+A_3)e^{-2k^*\eta}-\frac{1}{3k^*}(A_2+A_4)e^{-3k^*\eta}\right)_0^{\eta}}d\eta}}d\eta \tag{70}$$

$$\varphi(\eta)=\int_0^{\eta}e^{-Sc\left(R\eta+\frac{1}{k^*}(1+c)\eta+\frac{1}{(k^*)^2}(1+c)e^{-k^*\eta}+(A_1+A_3+2A_2+2A_4)\eta+\frac{1}{k^*}(2(A_1+A_3)+3(A_2+A_4))e^{-k^*\eta}-\frac{1}{2k^*}(A_1+A_3)e^{-2k^*\eta}-\frac{1}{3k^*}(A_2+A_4)e^{-3k^*\eta}\right)_0^{\eta}}d\eta \tag{71}$$

It is worth noting that Eqs. (11) and (12) subject to the associated boundary conditions may result in the following deduction if $\Pr = Sc$:

$$\theta_{WB}(\eta)-1=-\frac{\theta'_{WB}(0)}{N_b\theta'_{WoB}(0)}\left(e^{-N_b(\theta_{WoB}(\eta)-1)}-1\right),\ \frac{\theta'_{WB}(0)}{\theta'_{WoB}(0)}=\frac{N_b}{e^{N_b}-1} \tag{72}$$

In Eq. (72), indexes *WB* and *WoB* denote cases with regard to 'with Brownian motions' and 'without Brownian motions' respectively. It should be mentioned that such a deduction has been also previously noted by Jafarimoghaddam regarding the wall jet analysis for nanofluids (see [28]).

5. Numerical solution

4th-order Runge-Kutta is applied to discrete the coupled equations of momentum. An appropriate shooting technique is then used to convert the initially BVPs to IVPs. As mentioned, the rest of the transport equations are solved simply using a direct integration procedure. In order to proceed with R-K algorithm the involved equations were considered as:

$$F_1=f(\eta) \tag{73}$$

$$Y_1=F'_1 \tag{74}$$

$$Z_1=Y'_1 \tag{75}$$

$$F_2=g(\eta) \tag{76}$$

$$Y_2=F'_2 \tag{77}$$

$$Z_2=Y'_2 \tag{78}$$

$$Z'_1=\frac{-(M\beta+1)(F_1+F_2)Z_1+Y_1^2-\beta(2(F_1+F_2)Y_1Z_1)+(M+K)Y_1}{(1-\beta(F_1+F_2)^2)} \tag{79}$$

$$Z'_2=\frac{-(M\beta+1)(F_1+F_2)Z_2+Y_2^2-\beta(2(F_1+F_2)Y_2Z_2)+(M+K)Y_2}{(1-\beta(F_1+F_2)^2)} \tag{80}$$

Table 1
Comparison for $f''(0)$ and $g''(0)$.

	$f''(0)$/1st order HPM	$f''(0)$/2nd order HPM	$f''(0)$/R-K	$g''(0)$/1st order HPM	$g''(0)$/2nd order HPM	$g''(0)$/R-K
$\beta=0.25, K=M=R=0$						
c = 0.1	−1.0884	−1.09320	−1.09297	−0.08002	−0.07539	−0.07402
c = 0.5	−1.20041	−1.20860	−1.20139	−0.5313	−0.52502	−0.51299
c = 1	−1.34715	−1.35030	−1.33122	−1.34715	−1.35030	−1.33122
$\beta=0.5, K=M=R=0$						
c = 0.1	−1.15738	−1.16391	−1.16450	−0.08644	−0.08135	−0.07641
c = 0.5	−1.30515	−1.31647	−1.30489	−0.58185	−0.57556	−0.55413
c = 1	−1.5	−1.50670	−1.4710	−1.5	−1.50670	−1.4710
$\beta=1, K=M=R=0$						
c = 0.1	−1.28684	−1.29626	−1.29350	−0.09809	−0.09234	−0.08480
c = 0.5	−1.4954	−1.51270	−1.49263	−0.67239	−0.66672	−0.62825
c = 1	−1.76908	−1.78279	−1.72143	−1.76908	−1.78279	−1.72143
$K=0.25, \beta=M=R=0$						
c = 0.1	−1.13321	−1.13489	−1.13555	−0.0875	−0.08448	−0.08363
c = 0.5	−1.19689	−1.20045	−1.20004	−0.53545	−0.53046	−0.52677
c = 1	−1.27778	−1.27752	−1.27344	−1.27778	−1.27752	−1.27344
$K=0.5, \beta=M=R=0$						
c = 0.1	−1.23856	−1.23983	−1.24063	−0.10014	−0.09775	−0.09715
c = 0.5	−1.29636	−1.29893	−1.29854	−0.58926	−0.58474	−0.58164
c = 1	−1.37032	−1.36944	−1.36586	−1.37032	−1.36944	−1.36586
$K=1, \beta=M=R=0$						
c = 0.1	−1.42614	−1.42695	−1.42682	−0.12191	−0.12028	−0.12019
c = 0.5	−1.47573	−1.47720	−1.47694	−0.68516	−0.68150	−0.67993
c = 1	−1.5396	−1.53815	−1.53554	−1.5396	−1.53815	−1.53554
$K=\beta=M=R=0$, (Ref. [1])						
c = 0.1	−1.017027	−1.01939	−1.020260	−0.073099	−0.06913	−0.066847
c = 0.5	−1.088662	−1.09383	−1.093095	−0.476290	−0.47086	−0.465205
c = 1	−1.178511	−1.17933	−1.173721	−1.178511	−1.17933	−1.173721

Table 2
Comparison for $-\theta'(0)$.

	$c=1,\beta=M=K=R=N_b=0$			$c=0.5,\beta=M=K=R=N_b=0$			$c=0.1,\beta=M=K=R=N_b=0$		
	$-\theta'(0)$/1st order HPM	$-\theta'(0)$/2ndorder HPM	$-\theta'(0)$/ R-K	$-\theta'(0)$/1st order HPM	$-\theta'(0)$/2ndorder HPM	$-\theta'(0)$/ R-K	$-\theta'(0)$/1st order HPM	$-\theta'(0)$/2ndorder HPM	$-\theta'(0)$/ R-K
$Pr=0.5$	0.52604	0.5296	0.523	0.45323	0.45118	0.45106	0.37792	0.37763	0.37757
$Pr=1$	0.85427	0.85224	0.85214	0.73689	0.73538	0.73545	0.61819	0.61817	0.61816
$Pr=10$	3.30734	3.30813	3.30883	2.86014	2.86152	2.86148	2.43142	2.43241	2.43253
$Pr=20$	4.7883	4.7891	4.7905	4.1425	4.14441	4.14437	3.52879	3.53034	3.53022
$Pr=100$	11.0298	11.0332	11.0341	9.54758	9.55111	9.55101	8.15635	8.15888	8.15894
	$c=1,\beta=0.25,M=K=R=N_b=0$			$c=0.5,\beta=0.25,M=K=R=N_b=0$			$c=0.1,\beta=0.25,M=K=R=N_b=0$		
	$-\theta'(0)$/1st order HPM	$-\theta'(0)$/2ndorder HPM	$-\theta'(0)$/ R-K	$-\theta'(0)$/1st order HPM	$-\theta'(0)$/2ndorder HPM	$-\theta'(0)$/ R-K	$-\theta'(0)$/1st order HPM	$-\theta'(0)$/2ndorder HPM	$-\theta'(0)$/ R-K
$Pr=0.5$	0.48104	0.47312	0.47211	0.42317	0.41689	0.41588	0.35867	0.35399	0.35407
$Pr=1$	0.80382	0.79917	0.79716	0.7034	0.69934	0.69831	0.59661	0.59378	0.59341
$Pr=10$	3.26273	3.26512	3.26593	2.83071	2.83465	2.83263	2.41232	2.41238	2.41249
$Pr=20$	4.74594	4.75123	4.75052	4.11456	4.11761	4.11744	3.51069	3.51188	3.51142
$Pr=100$	10.9909	10.9956	10.9982	9.52191	9.52591	9.52676	8.1398	8.1401	8.142
	$c=1,K=0.25,M=\beta=R=N_b=0$			$c=0.5,K=0.25,M=\beta=R=N_b=0$			$c=0.1,K=0.25,M=\beta=R=N_b=0$		
	$-\theta'(0)$/1st order HPM	$-\theta'(0)$/2ndorder HPM	$-\theta'(0)$/ R-K	$-\theta'(0)$/1st order HPM	$-\theta'(0)$/2ndorder HPM	$-\theta'(0)$/ R-K	$-\theta'(0)$/1st order HPM	$-\theta'(0)$/2ndorder HPM	$-\theta'(0)$/ R-K
$Pr=0.5$	0.50833	0.50677	0.50605	0.43349	0.43218	0.43117	0.35710	0.35689	0.35669
$Pr=1$	0.83397	0.83312	0.8324	0.71409	0.71288	0.71262	0.59391	0.59388	0.59378
$Pr=10$	3.28592	3.28799	3.28755	2.83603	2.83651	2.83688	2.40561	2.40593	2.40639
$Pr=20$	4.76696	4.76891	4.76931	4.1185	4.11932	4.11972	3.50313	3.50482	3.50415
$Pr=100$	11.0086	11.0101	11.0131	9.52387	9.52663	9.52601	8.13099	8.13199	8.13289

6. Comparison

In this section, we briefly compare some results obtained via the purely analytic strategies presented here with those obtained numerically. In Table 1, values of $f''(0)$ and $g''(0)$ for some cases obtained analytically have been compared with those calculated numerically.

Table 2 shows a comparison between values of $\theta'(0)$ in different Prandtl numbers for several cases obtained by the analytic solutions and those quantified numerically.

According to the comparison outcome, it is easy to confirm that regarding the present highly nonlinear coupled equations, the parameter expansion technique (2nd order HPM) relatively fails to provide considerably more accurate results than the 1st order HPM respecting the studied range. In other words, accounting the computational cost, the 1st order HPM solution is much more appreciated. Therefore, we shall proceed with the visualization of the results in an extended form considering the 1st order HPM solution.

Table 3
Effect of the involved parameters on the factors of engineering interest.

$\beta\uparrow$ **or** $K\uparrow$ **or** $M\uparrow$ **or** $c\uparrow$ $\Rightarrow f''(0)\uparrow$**and** $g''(0)\uparrow$
$\beta\downarrow$ **or** $K\downarrow$ **or** $M\downarrow$ **or** $c\uparrow$ **or** $Sc\uparrow$ $\Rightarrow\phi'(0)\uparrow$
$\beta\downarrow$ **or** $K\downarrow$ **or** $M\downarrow$ **or** $c\uparrow$ **or** $Sc\downarrow$ **or** $N_b\downarrow$ **or** Pr $\uparrow$ $\Rightarrow\theta'(0)\uparrow$

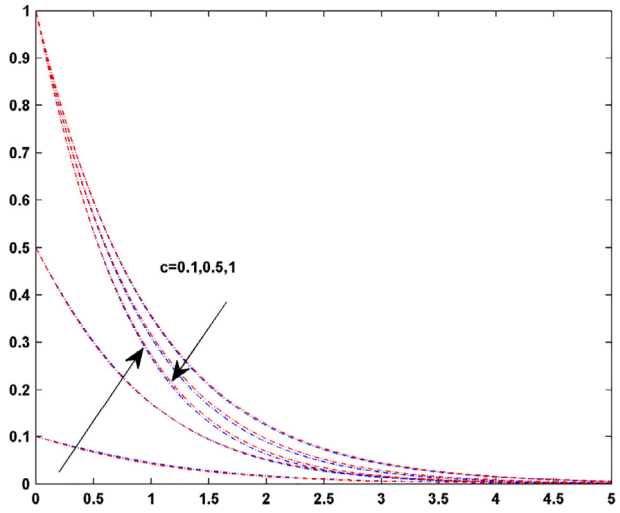

Fig. 5. Comparison of $f'(\eta)$ (upper) and $g'(\eta)$ (lower) obtained analytically, 1st order HPM (red) and numerically (blue) where $\beta=K=M=R=0$.

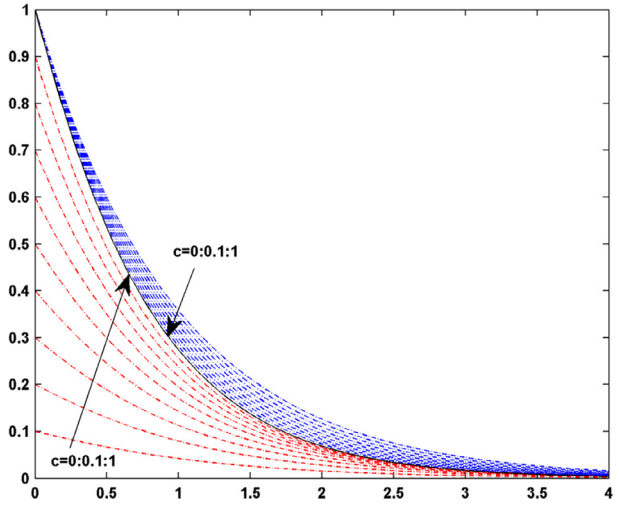

Fig. 6. velocity profiles ($f'(\eta)$ (blue) and $g'(\eta)$ (red)) where $\beta=M=K=0$.

Besides, Fig. 5 has been plotted to serve as a comparison between the two approaches (1st order HPM and numeric) for $f'(\eta)$ and $g'(\eta)$ in the pure Newtonian case.

It is worth mentioning that here; the proposed homotopy structure with the artificial perturbation parameter was constructed in such a way being easily expandable by the formal straightforward method (Taylor method). By choosing an amenable auxiliary linear operator as well as applying the rule of no-secular terms the truncated orders of the series solution could be simply obtained. Normally, by increasing the series terms, more accurate solutions are expected (as observed respecting the present nonlinearity); but undeniably, the convergence acceleration highly depends on the nature of the nonlinearity (as examined in the present research). Obviously, each nonlinear solver has its merits; e.g. HAM directly uses the Taylor method for expansion with no option to apply other existing perturbation techniques; besides, because the initial guess is not based on a firm principle, usually many series terms are applied to ensure an admissible convergence (in addition to securing the controlling parameter). Nevertheless, HAM could usually benefit from the convergence accelerating parameter leading to a very fast convergence in some problems; whilst, such a parameter does not exist in the classic HPM strategy (for more information see [29–34]).

7. Visualization and discussion

In this section, it is presented sufficient figures to express the quality of the obtained analytic solutions (1st order HPM). In the first place, it is referred to Table 3 which qualitatively shows the effect of the engaged parameters on the factors of engineering interest.

Figs. 6–8 express the behaviors of $f'(\eta)$ and $g'(\eta)$ in different stretching ratios (c) and in three different stations of $\beta = M = K = 0$, $\beta = K = 1, M = 0$ and $\beta = K = 1, M = 2$ respectively. According to these figures it is readily confirmed that increasing the stretching ratio results in enhancing both the zeroth values $f''(0)$ and $g''(0)$. Figs. 9–11 show the quantities of $f''(0)$ and $g''(0)$ as functions of stretching ratio in various Deborah numbers and for three stations of $M = K = 0$, $K = 1, M = 0$ and $M = 1, K = 0$ respectively. Examining the figures reveals a stronger effect by the imposed magnetic field compared to the Darcy porosity effect. Figs. 12–13 show the topographical view of $f''(0)$ and $g''(0)$ as functions of stretching ratio and Deborah number where $M = K = 0$. Based on these figures, the enhancing effect of Deborah

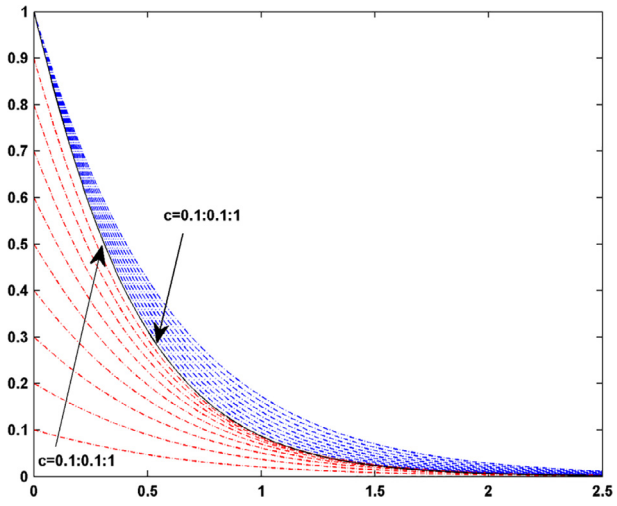

Fig. 7. velocity profiles ($f'(\eta)$ (blue) and $g'(\eta)$ (red)) where $\beta = K = 1, M = 0$.

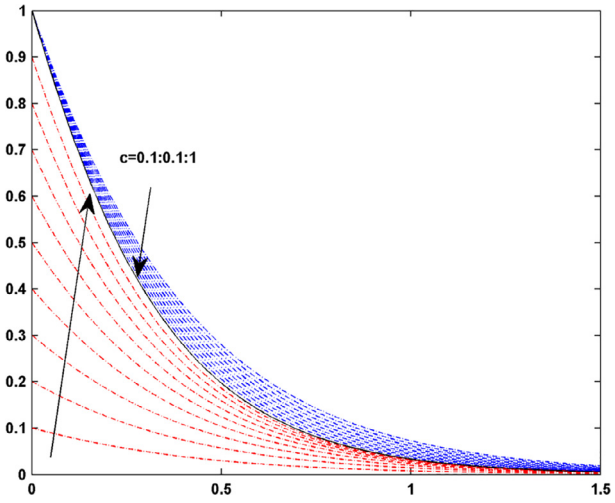

Fig. 8. velocity profiles ($f'(\eta)$ (blue) and $g'(\eta)$ (red)) where $\beta = K = 1, M = 2$.

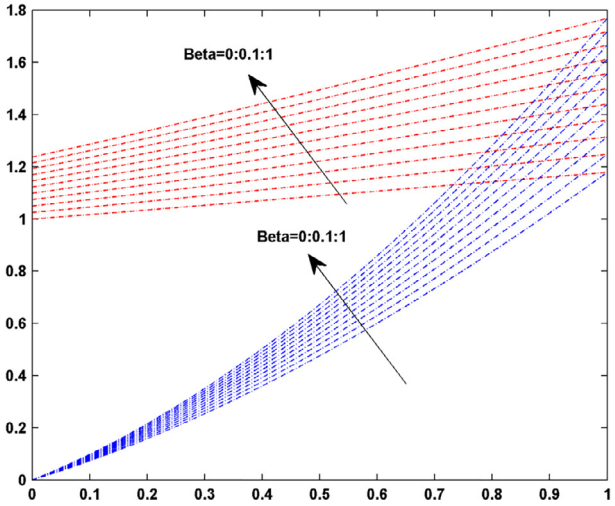

Fig. 9. values of $-f''(0)$ (red) and $-g''(0)$ (blue) as functions of stretching ratio (horizontal axis) where $M = K = 0$.

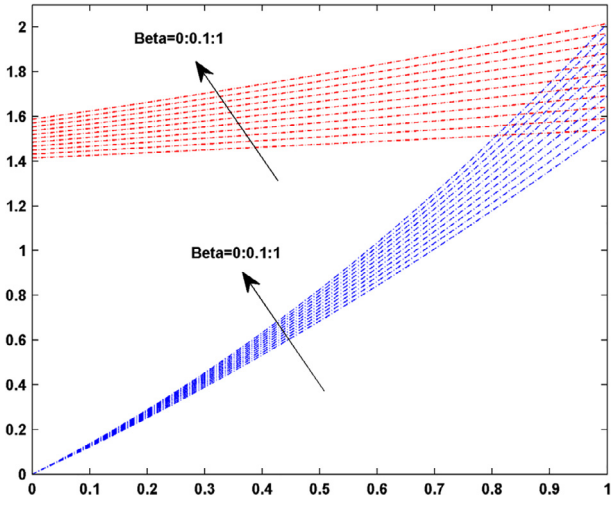

Fig. 10. values of $-f''(0)$ (red) and $-g''(0)$ (blue) as functions of stretching ratio (horizontal axis) where $K = 1, M = 0$.

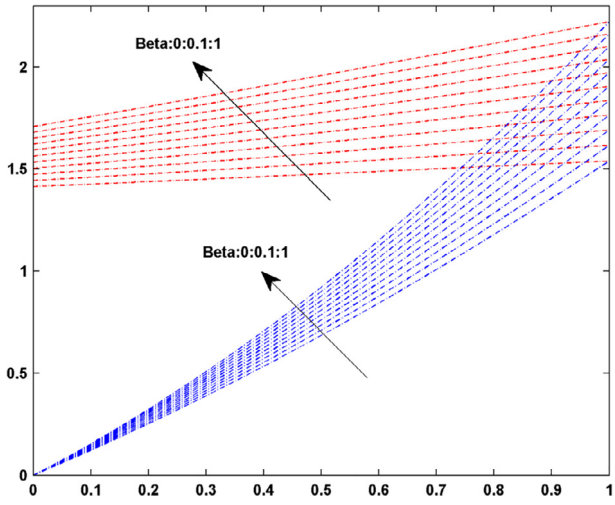

Fig. 11. values of $-f''(0)$ (red) and $-g''(0)$ (blue) as functions of stretching ratio (horizontal axis) where $K = 0, M = 1$.

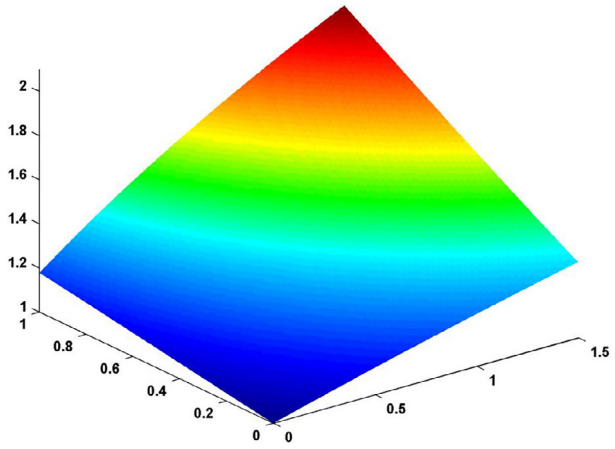

Fig. 12. topographical view of $-f''(0)$ as a function of c and β where $M = K = 0$; $0 \leqslant c \leqslant 1$ and $0 \leqslant \beta \leqslant 1.5$.

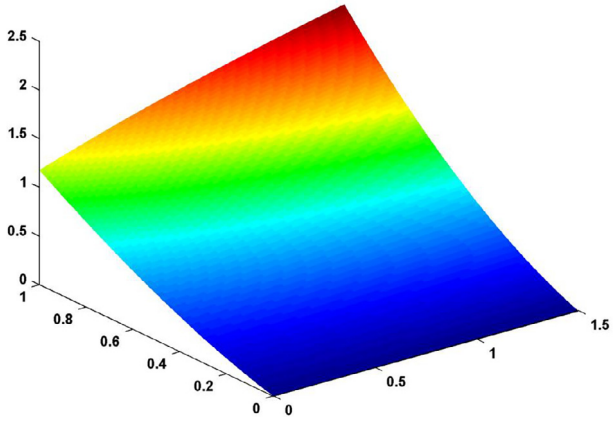

Fig. 13. topographical view of $-g''(0)$ as a function of c and β where $M = K = 0$; $0 \leqslant c \leqslant 1$ and $0 \leqslant \beta \leqslant 1.5$.

number on the normalized skin friction coefficient is evident. In other words, by getting further from the Newtonian fluids (being in accordance with the UCM constitutional model) the values of engineering interest rise accordingly. Figs. 14–15 betray the concentration profiles in various stretching ratios and with respect to three stages of $Sc = 0.5$, $Sc = 1$ and $Sc = 2$ where the hydrodynamic factors are $\beta = M = K = 0$ and $\beta = K = 1.5, M = 0$ respectively. As shown in Table 3, by increasing Schmidt number, an increase within the normalized Sherwood number is expected. In Fig. 16, the topographical view of $\phi'(0)$ is depicted as a function of stretching ratio and porosity parameter where the magnetic parameter and Deborah number are equal to zero and $Sc = 1$. Fig. 17 shows analogous quantity as a function of stretching ratio and Deborah number where the both factors associated with magnetic and porosity effects are zero. Fig. 18 shows$\phi'(0)$ as a function of Deborah number and magnetic parameter where $Sc = 10$ and $K = 0$ and flow is axisymmetric. This figure shows that both the magnetic parameter and Deborah number express minor effects

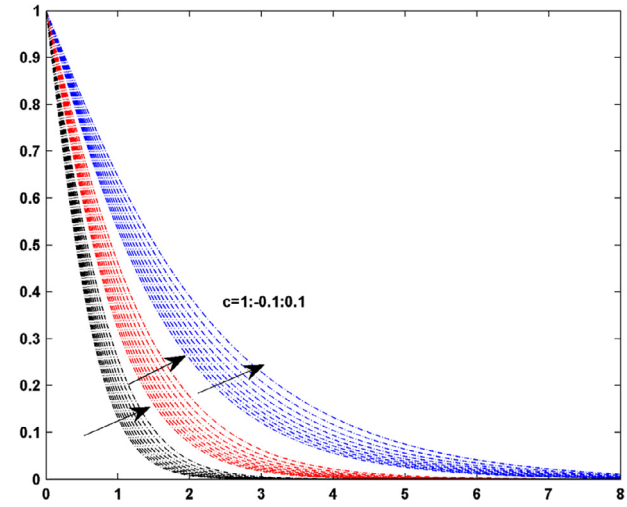

Fig. 14. $\phi(\eta)$ where $\beta = M = K = 0$ (blue: $Sc = 0.5$, red: $Sc = 1$, black: $Sc = 2$).

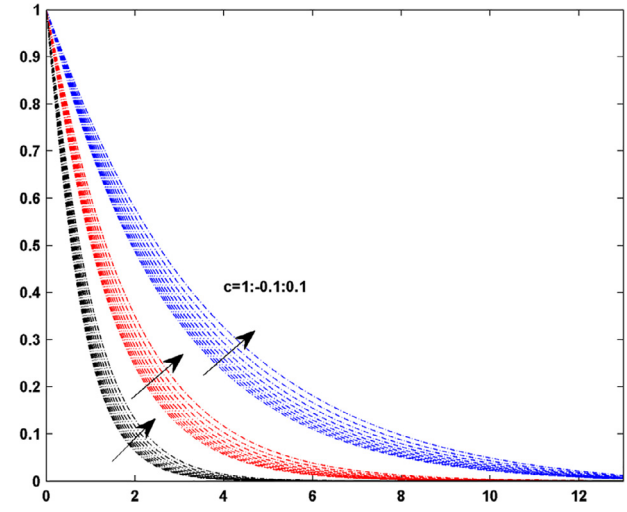

Fig. 15. $\phi(\eta)$ where $\beta = K = 1.5, M = 0$ (blue: $Sc = 0.5$, red: $Sc = 1$, black: $Sc = 2$).

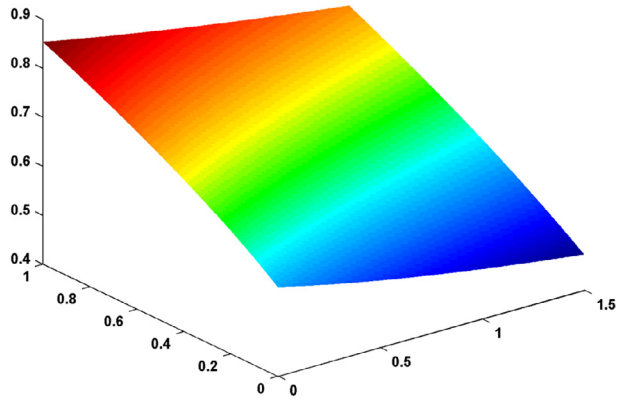

Fig. 16. topographical view of $-\phi'(0)$ as a function of K and c where $M=\beta=0, Sc=1$; $0\leqslant c\leqslant 1$ and $0\leqslant K\leqslant 1.5$.

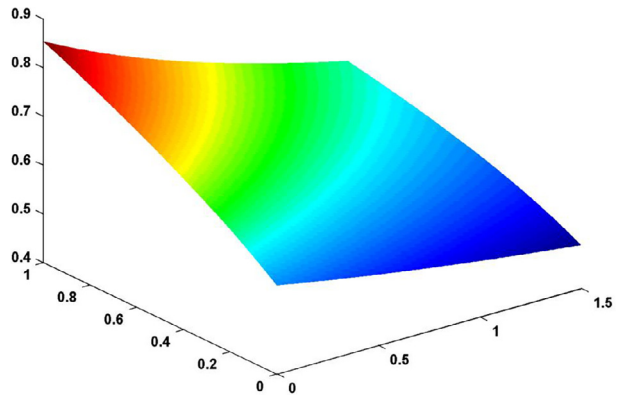

Fig. 17. topographical view of $-\phi'(0)$ as a function of β and c where $M=K=0, Sc=1$; $0\leqslant c\leqslant 1$ and $0\leqslant \beta\leqslant 1.5$.

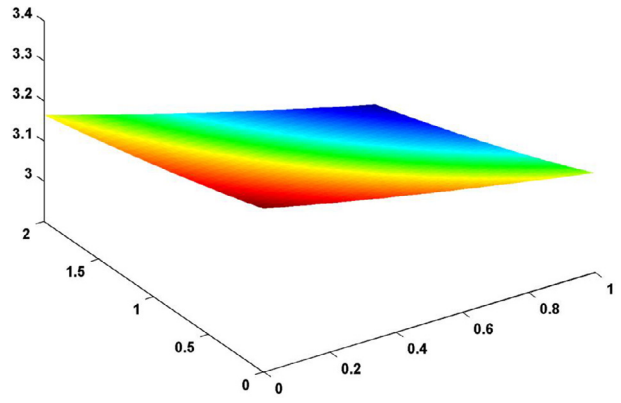

Fig. 18. topographical view of $-\phi'(0)$ as a function of β and M where $K=0, Sc=1, c=1$; $0\leqslant \beta\leqslant 1$ and $0\leqslant M\leqslant 2$.

on the normalized Sherwood number respecting the studied ranges. Fig. 19 illustrates $\phi'(0)$ as a function of Schmidt number and stretching ratio where $\beta=M=K=0$. Figs. 20–22 show the temperature profiles in various values of stretching ratio and in different stages of $\Pr=0.5$, $\Pr=1$ and $\Pr=2$ where $Sc=1$ and in three stations of $\beta=K=M=0, N_b=10$, $\beta=K=M=0, N_b=1$ and $\beta=K=1, M=0, N_b=1$ respectively. Figs. 23–26 show topographical view of the normalized convective heat transfer coefficient $\theta'(0)$ as functions of N_b, c, Sc, c, β, c and $\Pr, c$ respectively. It

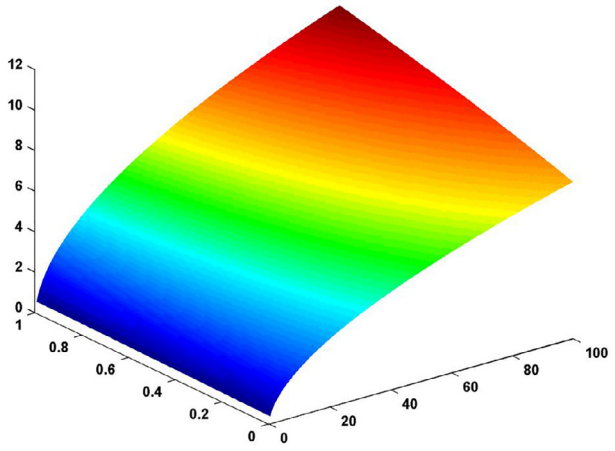

Fig. 19. topographical view of $-\phi'(0)$ as a function of Sc and c where $K=M=\beta=0$; $0\leqslant c\leqslant 1$ and $0.5\leqslant Sc\leqslant 100$.

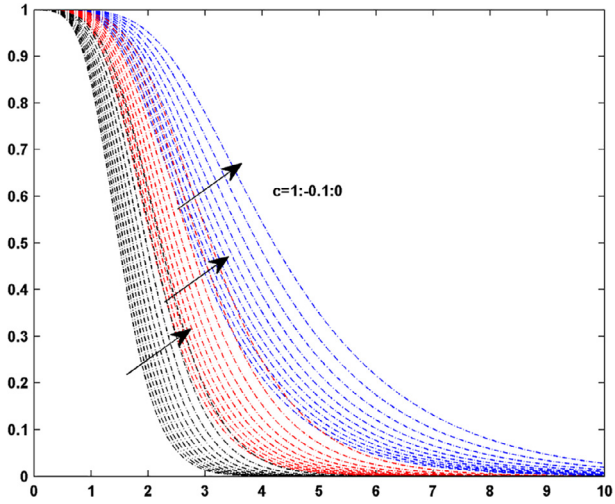

Fig. 20. $\theta(\eta)$ where $\beta=K=M=0, Sc=1, N_b=10$ (blue: $\Pr=0.5$, red: $\Pr=1$, black: $\Pr=2$).

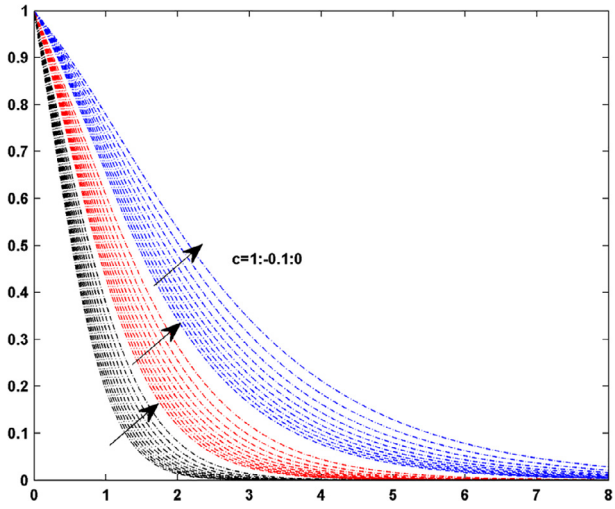

Fig. 21. $\theta(\eta)$ where $\beta=K=M=0, Sc=1, N_b=1$ (blue: $\Pr=0.5$, red: $\Pr=1$, black: $\Pr=2$).

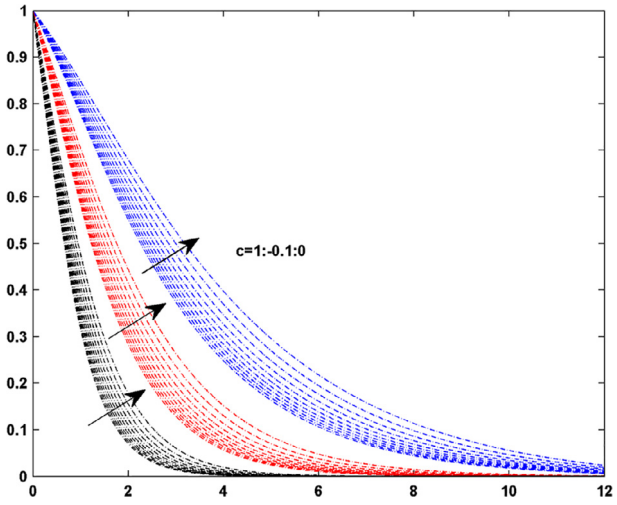

Fig. 22. $\theta(\eta)$ where $\beta = K = 1, M = 0, Sc = 1, N_b = 1$ (blue: Pr = 0.5, red: Pr = 1, black: Pr = 2).

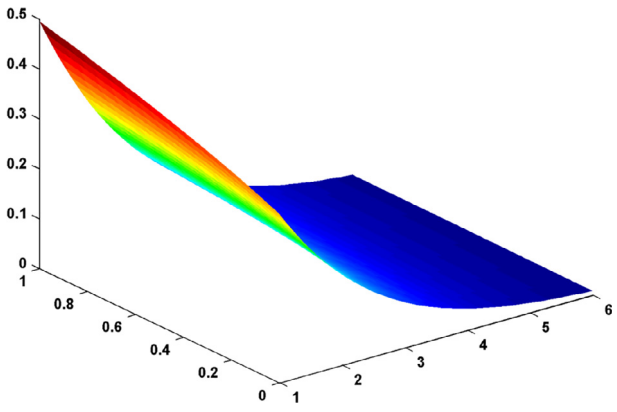

Fig. 23. $-\theta'(0)$ where $\beta = K = M = 0, Sc = \Pr = 1;\ 0 \leqslant c \leqslant 1,\ 1 \leqslant N_b \leqslant 6$.

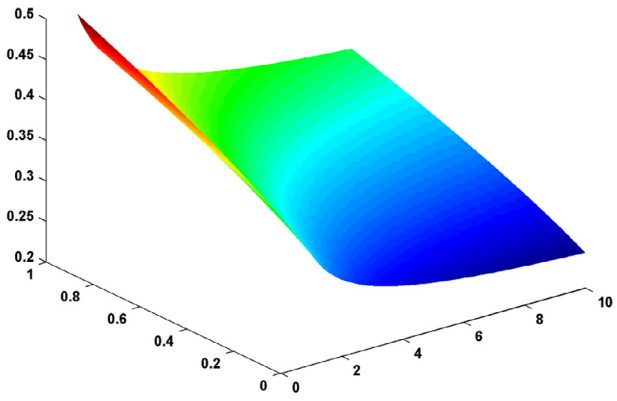

Fig. 24. $-\theta'(0)$ where $\beta = K = M = 0, N_b = \Pr = 1;\ 0 \leqslant c \leqslant 1,\ 1 \leqslant Sc \leqslant 10$.

is of worth mentioning that by increasing the Brownian heat diffusion parameter the normalized convective heat transfer coefficient shrinks rather drastically. Please note that Table 3 is sufficient to justify all the trends observed respecting the presented figures. Therefore, here we are not to repeat the observed trends separately for each individual case. It is only additionally stated that in the

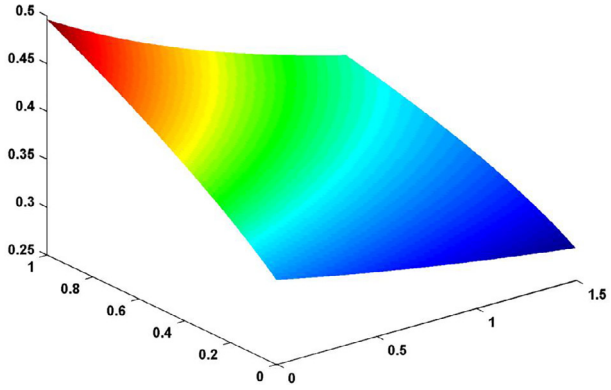

Fig. 25. $-\theta'(0)$ where $K = M = 0, N_b = \Pr = Sc = 1;\ 0 \leqslant c \leqslant 1,\ 0 \leqslant \beta \leqslant 1.5$.

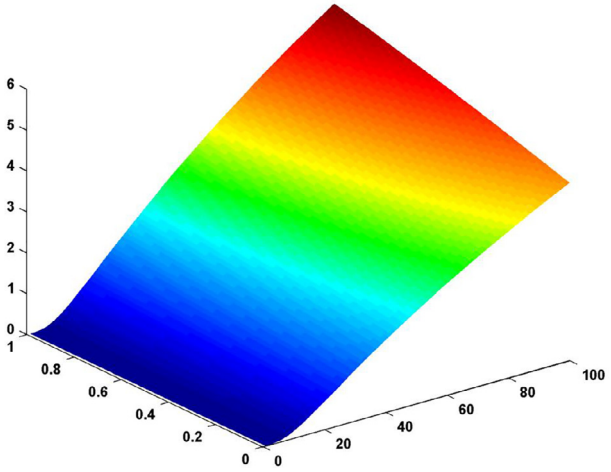

Fig. 26. $-\theta'(0)$ where $K = M = \beta = 0, N_b = Sc = 10;\ 0 \leqslant c \leqslant 1,\ 1 \leqslant \Pr \leqslant 100$.

usual range of the hydrodynamic factors of β, K and M, almost no considerable effect on either $\phi'(0)$ or $\theta'(0)$ can be observed (e.g. see Fig. 18). Finally, for the purely Newtonian case ($\beta = M = K = 0$) where $N_b = 0$, the following correlation can be derived from the HPM results to predict the normalized convective heat transfer coefficient:

$$-\theta'(0) = 0.7425\Pr^{0.5178}(c + 0.9244)^{0.4786},\ \Pr \geqslant 10,\ R - square \approx 1 \tag{81}$$

It should be mentioned that obviously Eq. (81) can be also applied for calculating $\phi'(0)$. Further note that this correlation falls into deviation if Prandtl number is extremely large. To admit such a statement, it is easy to note that if $c = 0$ the problem turns to the two-dimensional stretching sheet flow (in which the well-known closed form solution for $\theta'(0)$ is in the form of incomplete gamma function) where it can be simply shown asymptotically that $\theta'(0)|\Pr \to \infty \propto \Pr^{0.5}$. This is whilst Eq. (81) reveals $\theta'(0)|\Pr \to \infty \propto \Pr^{0.5178}$.

Now, the origin of such a deviation in extremely large Prandtl numbers becomes clear

8. Conclusion

It was studied three-dimensional MHD/Porous Maxwell nanofluids due to a bidirectional stretching surface. The problem became a bit simplified since the thermophoresis effect was ignored. He's homotopy perturbation method of the 1st and 2nd

orders were applied to solve the resulting similarity equations of momentum. For the range of the studied parameters, the agreement between the analytic results and those obtained numerically was shown to be remarkable. It was then moved forward to solve the rest of the transport equations simply by a numerical integration procedure. It was visualized the effect of the engaged parameters in a comprehensive manner. Furthermore, a correlation was derived to predict Nusselt number for Newtonian case with $N_b = 0$ where the effects imposed due to the presence of magnetic field and porosity were ignored.

Conflict of interest

There is no competing interest of any kind within this submission.

Authors' contribution

AJ is the sole author of the present paper.

References

[1] P. Donald Ariel, Generalized three-dimensional flow due to a stretching sheet, ZAMM ·Z. Angew. Math. Mech. 83 (12) (2003) 844–852, https://doi.org/10.1002/zamm.200310052.

[2] P.D. Ariel, On computation of the three-dimensional flow past a stretching sheet, Appl. Math. Comput. 188 (2007) 1244–1250.

[3] Xu. Hang, Shi-Jun Liao, Ioan Pop, Series solutions of unsteady three-dimensional MHD flow and heat transfer in the boundary layer over an impulsively stretching plate, Eur. J. Mech. B/Fluids 26 (2007) 15–27.

[4] T. Hayat, T. Javed, On analytic solution for generalized three-dimensional MHD flow over a porous stretching sheet, Phys. Lett. A 370 (2007) 243–250.

[5] T. Hayat, M. Sajidb, I. Pop, Three-dimensional flow over a stretching surface in a viscoelastic fluid, Nonlinear Anal. Real World Appl. 9 (2008) 1811–1822.

[6] T. Hayat, M. Awais, Three-dimensional flow of upper-convected Maxwell (UCM) fluid, Int. J. Numer. Meth. Fluids 66 (2011) 875–884.

[7] T. Hayat, S.A. Shehzad, A. Alsaedi, M.S. Alhothuali, Three-dimensional flow of Oldroyd-B fluid over surface with convective boundary conditions, Appl. Math. Mech. -Engl. Ed. 34 (4) (2013) 489–500.

[8] T. Hayat, Taseer Muhammad, S.A. Shehzad, G.Q. Chen, Ibrahim A. Abbas, Interaction of magnetic field in flow of Maxwell nanofluid with convective effect, J. Mag. Mag. Mater. (2015), https://doi.org/10.1016/j.jmmm.2015.04.019.

[9] G.K. Ramesh, B.C. Prasannakumara, B.J. Gireesha, S.A. Shehzad, F.M. Abbasi, Three dimensional flow of Maxwell fluid with suspended nanoparticles past a bidirectional porous stretching surface with thermal radiation, Therm. Sci. Eng. Progress 1 (2017) 6–14.

[10] M. Awais, T. Hayat, A. Alsaedi, S. Asghar, Time-dependent three-dimensional boundary layer flow of a Maxwell fluid, Comput. Fluids 91 (2014) 21–27.

[11] T. Hayat, M. Awais, S. Obaidat, Three-dimensional flow of a Jeffery fluid over a linearly stretching sheet, Commun. Nonlinear Sci. Numer. Simul. 17 (2012) 699–707.

[12] M. Bilal Ashraf, T. Hayat, M.S. Alhuthali, Three-dimensional flow of maxwell fluid with soret and dufour effects, Am. Soc. Civil Eng. (2015), https://doi.org/10.1061/(ASCE)AS.1943-5.0000551.

[13] S. Bilal, Khalil-ur-Rehman, M.Y. Malik, Arif Hussain, Mair Khan, Effects of temperature dependent conductivity and absorptive/generative heat transfer on MHD three dimensional flow of Williamson fluid due to bidirectional non-linear stretching surface, Res. Phys. 7 (2017) 204–212.

[14] S.A. Shehzad, A. Alsaedi, T. Hayat, Hydromagnetic steady flow of maxwell fluid over a bidirectional stretching surface with prescribed surface temperature and prescribed surface heat flux, PLoS ONE 8 (7) (2013) e68139, https://doi.org/10.1371/journal.pone.0068139.

[15] J.A. Khan, M. Mustafa, T. Hayat, M. Sheikholeslami, A. Alsaedi, Three-Dimensional Flow of Nanofluid Induced by an Exponentially Stretching Sheet: An Application to Solar Energy, PLoS ONE 10 (3) (2015) e0116603, https://doi.org/10.1371/journal.pone.0116603.

[16] T. Hayat, S.A. Shehzad, A. Alsaedi, MHD three-dimensional flow of Maxwell fluid with variable thermal conductivity and heat source/sink, International, J. Numer. Methods Heat Fluid Flow 24 (5) (2014) 1073–1085.

[17] S. Saleem, M. Awais, S. Nadeem, N. Sandeep, T. Mustafa, Theoretical analysis of upper-convected Maxwell fuid fow with Cattaneo-Christov heat flux model, Chin. J. Phys. (2017), https://doi.org/10.1016/j.cjph.2017.04.005.

[18] Tasawar Hayat, Arsalan Aziz, Taseer Muhammad, Ahmed Alsaedi, Three-dimensional flow of nanofluid with heat and mass flux boundary conditions, Chin. J. Phys. 55 (2017) 1495–1510.

[19] Z.H. Khan, M. Qasim, Rizwan Ul Haq, Qasem M. Al-Mdallal, Closed form dual nature solutions of fluid flow and heat transfer over a stretching/shrinking sheet in a porous medium, Chinese J. Phys. 55 (2017) 1284–1293.

[20] M. Bilal et al., Three dimensional MHD upper-convected Maxwell nanofluid flow with nonlinear radiative heat flux, Alexandria Eng. J. (2017), https://doi.org/10.1016/j.aej.2017.03.039.

[21] L. Xu, He's homotopy perturbation method for a boundary layer equation in unbounded domain, Comput Math Appl 54 (2007) 1067–1070.

[22] J.H. He, Periodic solutions and bifurcations of delay-differential equations, Phys Lett A 347 (2005) 228–230.

[23] J.H. He, An elementary introduction to the homotopy perturbation method, Comput Math Appl 57 (2009) 410–412.

[24] J. Buongiorno, Convective transport in nanofluids, J. Heat Transfer 128 (3) (2005) 240–250.

[25] A. Sohail, S.I.A. Shah, W.A. Khan, M. Khan, Thermally radiative convective flow of magnetic nanomaterial: A revised model, doi.org/10.1016/j.rinp.2017.07.011.

[26] Masood Khan, Waqar Azeem Khan, MHD boundary layer flow of a power-law nanofluid with new mass flux condition, AIP Adv. 6 (2016) 025211, https://doi.org/10.1063/1.4942201.

[27] J.H. He, Comparison of homotopy perturbation and homotopy analysis method, Appl. Math. Comput. 156 (2004) 527–539.

[28] Amin Jafarimoghaddam, Closed form analytic solutions to heat and mass transfer characteristics of wall jet flow of nanofluids, Thermal Science and Engineering Progress 4 (2017) 175–184.

[29] M. Turkyilmazoglua, Some issues on HPM and HAM methods: a convergence scheme, Math Comput Model 53 (9–10) (2011) 1929–1936.

[30] M. Turkyilmazoglua, An effective approach for approximate analytical solutions of the damped duffing equation, Phys Scripta 86 (1) (2012).

[31] Amin Jafarimoghaddam, Hossein Aberoumand, Sadegh Aberoumand, Ali Akbar Abbasian Arani, Ali Habibollahzade, MHD wedge flow of nanofluids with an analytic solution to an especial case by Lambert W-function and Homotopy Perturbation Method, Eng. Sci. Technol., Int. J. 20 (2017) 1515–1530.

[32] M. Turkyilmazoglua, An effective approach for evaluation of the optimal convergence control parameter in the homotopy analysis method, FILOMAT 30 (2016) 1633–1650.

[33] M. Turkyilmazoglu, is homotopy perturbation method the traditional Taylor series expansion, Hacettepe J. Math. Stat. 44 (3) (2015) 651–657.

[34] M. Turkyilmazoglu, Parametrized Adomian decomposition method with optimum convergence, Trans. Modell. Comput. Simul. 27 (4) (2017), https://doi.org/10.1145/3106373.